



# Cortex Thickness Is Key for the Colors of Iridescent Starling Feather Barbules With a Single, Organized Melanosome Layer

Pascal Freyer<sup>1†</sup>, Bodo D. Wilts<sup>2†</sup> and Doekele G. Stavenga<sup>1\*†</sup>

<sup>1</sup> Zernike Institute for Advanced Materials, University of Groningen, Groningen, Netherlands, <sup>2</sup> Adolphe Merkle Institute, University of Fribourg, Fribourg, Switzerland

## OPEN ACCESS

### Edited by:

Ahu Gumrah Dumanli-Parry,  
The University of Manchester,  
United Kingdom

### Reviewed by:

Hugo Gruson,  
University of London, United Kingdom  
Rox Middleton,  
University of Bristol, United Kingdom

### \*Correspondence:

Doekele G. Stavenga  
D.G.Stavenga@rug.nl

### †ORCID:

Pascal Freyer  
[orcid.org/0000-0002-9581-4693](https://orcid.org/0000-0002-9581-4693)  
Bodo D. Wilts  
[orcid.org/0000-0002-2727-7128](https://orcid.org/0000-0002-2727-7128)  
Doekele G. Stavenga  
[orcid.org/0000-0002-2518-6177](https://orcid.org/0000-0002-2518-6177)

### Specialty section:

This article was submitted to  
Behavioral and Evolutionary Ecology,  
a section of the journal  
Frontiers in Ecology and Evolution

**Received:** 23 July 2021

**Accepted:** 26 October 2021

**Published:** 19 November 2021

### Citation:

Freyer P, Wilts BD and  
Stavenga DG (2021) Cortex  
Thickness Is Key for the Colors  
of Iridescent Starling Feather Barbules  
With a Single, Organized Melanosome  
Layer. *Front. Ecol. Evol.* 9:746254.  
doi: 10.3389/fevo.2021.746254

The iridescent plumage of many birds is structurally colored due to an orderly arrangement of melanosomes in their feather barbules. Here, we investigated the blue-to purple-colored feathers of the European starling (*Sturnus vulgaris*) and the blue and green feathers of the Cape starling (*Lamprotornis nitens*). In both cases, the barbules contain essentially a single layer of melanosomes, but in *S. vulgaris* they are solid and rod-shaped, and in *L. nitens* they are hollow and rod- as well as platelet-shaped. We analyzed the coloration of the feathers by applying imaging scatterometry, bifurcated-probe- and micro-spectrophotometry. The reflectance spectra of the feathers of the European starling showed multiple peaks and a distinct, single peak for the Cape starling feathers. Assuming that the barbules of the two starling species contain a simple multilayer, consisting locally only of a cortex plus a single layer of melanosomes, we interpret the experimental data by applying effective-medium-multilayer modeling. The optical modeling provides quantitative insight into the function of the keratin cortex thickness, being the principal factor to determine the peak wavelength of the reflectance bands; the melanosome layer only plays a minor role. The air cavity in the hollow melanosomes of the Cape starling creates a strongly enhanced refractive index contrast, thus very effectively causing a high reflectance.

**Keywords:** refractive index, effective medium approach, multilayer modeling, keratin, melanin, directional reflectance

## INTRODUCTION

Many bird species feature a brightly colored plumage due to wavelength-selective absorbing pigments and/or more or less orderly arranged nano-scale structures (Durrer, 1977; Hill and McGraw, 2006; Kinoshita, 2008). A frequently occurring pigment in organisms is melanin, which causes, for example, the black feather colors of numerous bird species (McGraw, 2006) and has recently also attracted attention in bio-inspired materials (Xiao et al., 2020). In feathers of passerines that are colored by carotenoids, or parrot feathers colored by psittacofulvins, melanin functions to enhance color contrast by absorbing stray light that would otherwise desaturate the coloration (Tinbergen et al., 2013). Melanin has a similar contrast-enhancing function in feather barbs that

are structural colored due to nano-sized, spongy keratin structures (Prum, 2006; D'Alba et al., 2012; Tinbergen et al., 2013; Shawkey and D'Alba, 2017).

Remarkably, however, instead of being an effective absorber of light, melanised organelles (the melanosomes) can function as reflectors, because melanin has a relatively high refractive index ( $\sim 1.75$ ) with respect to the bulk feather material, keratin ( $\sim 1.55$ ; Mason, 1923; Durrer, 1977; Stavenga et al., 2015). When the melanosomes are contiguously packed in layers that alternate with keratin layers, they form optical multilayers in the barbules that highly reflect incident light within a restricted wavelength-range (Kinoshita, 2008). Striking examples where multilayers of solid melanin rodlets create bright reflectors include the feathers of birds-of-paradise (Durrer, 1977; Stavenga et al., 2011), common bronzewing pigeons (Xiao et al., 2014), and ducks (Eliason and Shawkey, 2012; Stavenga et al., 2017).

Air has a much lower refractive index than keratin, which causes a means to increase the refractive index contrast in a reflecting structure in feathers and therefore offers an attractive way to enhance their reflectance. For example, barbules with hollow melanin rodlets arranged in multilayers occur in turkey, magpie, and trogons (Durrer and Villiger, 1966; Eliason et al., 2013; Stavenga et al., 2018). Similarly, barbules with stacks of melanosomes that resemble hollow platelets generate the bright colors in many hummingbird feathers (Greenewalt et al., 1960; Durrer, 1977; Giraldo et al., 2018; Gruson et al., 2019; Eliason et al., 2020). In the unique case of peacock feathers, rectangular lattices of melanin rodlets and air channels embedded in the keratin matrix create highly reflecting barbules (Durrer, 1986). The rainbow of different colors of peacock feathers is realized by small variations in the dimensions of the lattice of air channels and melanin rodlets (Durrer, 1965; Zi et al., 2003; Freyer et al., 2019).

In the course of our studies on peacock feathers, we found that a crucial element of the peacock's photonic structures is the keratin cortex, a superficial layer of keratin overlying the layer of melanosomes. When the number of melanin and air channel layers is high, the cortex thickness has a minor effect on the reflectance spectrum of the barbules, but when the number of layers decreases, the cortex thickness becomes increasingly important (Freyer and Stavenga, 2020). We therefore decided to study the role of the cortex in greater detail in the limiting case where only a single layer of melanosomes exists. This is realized in the barbules of the colored feathers that are interspersed in the general blackish plumage of the European or Common starling, *Sturnus vulgaris*. Its melanin granules are solid rodlets (Durrer and Villiger, 1970). In the feather barbules of the Cape starling, *Lamprolornis nitens*, because of its exceptionally directional appearance also called the Cape glossy starling, a single layer of hollow, platelet-shaped melanosomes exists below a keratin cortex (Durrer and Villiger, 1970).

Here we investigate the effect of the different melanosome monolayers on the feather reflection properties of the two starling species. We calculate the reflectance spectra with an effective-medium-multilayer model based on realistic anatomical data and compare the results with optical measurements. We conclude that, for feather barbules with a single layer of melanosomes,

the thickness of the cortex is the most important parameter that determines the feather color and that the characteristics of the melanosome layer are of secondary importance. The air cavity in the melanosomes of the Cape starling considerably enhances the reflectance and thus the feather coloration.

## MATERIALS AND METHODS

### Starling Feather Samples and Images

Feathers were collected from dead specimens of *S. vulgaris* (in the Netherlands, near Groningen) and *L. nitens* (in Namibia, near Windhoek). Photomicrographs were made with a Canon EOS 30D camera. Micrographs of single barbules were made with a Zeiss Universal microscope (Zeiss AG, Oberkochen, Germany) equipped with a Zeiss Epiplan 40  $\times$  /0.85 objective and a ScopeTek DCM510 camera. A Zeiss 100  $\times$  /1.3 oil immersion objective was used for visualizing the melanosomes.

### Anatomy

Transmission electron microscopy (TEM) studies showed that the melanosomes of *S. vulgaris* are solid rodlets with a length of 1.2–1.7  $\mu\text{m}$  and diameter of 0.250–0.254  $\mu\text{m}$  (Durrer and Villiger, 1970). The hollow and platelet-shaped melanosomes found in the feather barbules of *Lamprolornis* species have a diameter of about 1.0  $\mu\text{m}$  by 0.8  $\mu\text{m}$  and a thickness of about 210–240 nm, because of two melanin layers of 70 nm and an intermittent air layer of 73–98 nm [as provided by Durrer and Villiger (1970); see also **Supplementary Tables 1, 2**]. We compared these values with data deduced from epi-illumination micrographs of barbules immersed in oil as well as with scanning electron micrographs (SEM) of the barbules (**Figures 2C, 6C**). We measured  $>30$  of the *S. vulgaris* melanosome rodlet widths from six different barbule cells from different barbs of a feather.

For SEM, small feather pieces were deposited on an aluminum SEM stub (Plano-EM, Wetzlar, Germany) covered with conductive carbon tape and subsequently sputter-coated with a 5 nm thick layer of gold, using a Cressington 208 HR sputter coater (Cressington Scientific Instruments, Watford, England). Additionally, silver paste was added to part of the feather piece to increase the conductivity of the sample, limit charging effects and provide a protecting envelope to limit curtaining effects when cutting the barbule. Electron microscope images were taken using a Thermo Scientific Scios 2 (FEI, Eindhoven, Netherlands) focused ion-beam scanning electron microscope (FIB-SEM). On-view images were recorded using the built-in Everhart-Thornley detector (ETD) with an electron beam current of 5 kV. To image the cross-section of the barbules, barbules embedded in silver paste were milled with the Ga-ion beam with 30 kV acceleration voltage and 1 nA beam current. Tilt-corrected images were acquired using the ETD and a beam current of 2 kV.

### Multilayer Modeling

The starling barbules were treated as a simple multilayer in air consisting of a keratin cortex and a melanosome layer embedded in keratin. We calculated reflectance spectra for

normal illumination using a transfer matrix program, written in Matlab code, based on classical optical multilayer theory (Yeh, 2005; Stavenga, 2014). An effective medium approach was chosen as these are often more intuitive and computationally accessible than full wave simulations, as performed below. The effective refractive index of the layer with melanosomes was obtained by:

$$\tilde{n}_{\text{eff}} = (f_k n_k^w + f_m \tilde{n}_m + f_a n_a^w)^{1/w} \quad (1)$$

where  $f_k$ ,  $f_m$ , and  $f_a$ , are the volume fractions of the keratin, melanin, and air components, with  $f_k + f_m + f_a = 1$ ;  $w$  is a weighting factor. The implemented refractive index of keratin was assumed to be pure dielectric with  $n_k = A_k + B_k \lambda^{-2}$  with  $A_k = 1.532$  and  $B_k = 5890 \text{ nm}^2$ , as keratin absorption in the visible is negligible (Leertouwer et al., 2011). The applied refractive index of melanin was complex:  $\tilde{n}_m = n_m - ik_m$  where  $n_m = A_m + B_m \lambda^{-2}$  and  $k_m = a_m \exp(-\lambda/b_m)$ , with  $A_m = 1.648$ ,  $B_m = 23700 \text{ nm}^2$ ,  $a_m = 0.56$ , and  $b_m = 270 \text{ nm}$  (Stavenga et al., 2015); the refractive index of air is wavelength-independent, with  $n_a = 1$ . In the case of solid melanosomes (*S. vulgaris*), the effective refractive index of the melanosome layer was calculated with  $f_a = 0$ . In a previous study on magpie feather barbules with stacked hollow melanosomes, a weighting factor  $w$  varying between  $-2.0$  and  $2.0$  was found to have distinct effects on the calculated reflectance spectra (Stavenga et al., 2018; similar effects occur in peacock barbules, see Freyer et al., 2019). However, in the present cases of barbules with a single melanosome layer, the reflectance spectra calculated for various values of  $w$  were very similar, and therefore all results presented here were obtained with a weighting factor  $w = 1$ .

To ascertain the validity of the effective medium approach, we furthermore performed for a few cases FDTD modeling, using Ansys Lumerical R2021.1 (see **Supplementary Figures 1, 2**). For these simulations, an idealized structured multilayer of keratin and melanin was placed in a 2D simulation box with a length of  $2 \mu\text{m}$  and a width determined by the modeled melanosome with periodic boundary conditions along the structure dimensions and perfectly matched layers (PMLs) in the direction of light illumination. The illumination was a linearly polarized, broadband light source (300–900 nm). A reflection monitor placed behind the light source measured the reflectance.

## Imaging Scatterometry

The spatial reflection of the barbules was visualized by imaging scatterometry (ISM). An isolated barbule was glued to the tip of a glass micropipette (Stavenga et al., 2009; Wilts et al., 2009). A narrow-aperture ( $< 5^\circ$ ) white-light beam was focused on a small circular area (diameter  $13 \mu\text{m}$ ) of a single barbule cell and the spatial distribution of the far-field scattered light was then monitored. The exposure times were adjusted to obtain a sufficiently clear image without overexposure.

## Spectrophotometry

Reflectance spectra of different areas of the starling feathers, about 2 mm in diameter, were measured with a bifurcated reflection probe (Avantes FCR-7UV200), using a CCD detector array spectrometer (Avantes AvaSpec-2048, Apeldoorn,

Netherlands). The light source was a deuterium-halogen lamp (Avantes AvaLight-D(H)-S), and the reference was a white diffusely scattering reflection tile (Avantes WS-2). Reflectance spectra of small barbule areas were measured with a microspectrophotometer (MSP). The MSP was a Leitz Ortholux microscope (Leitz, Wetzlar, Germany) with a LUCPlanFL  $20 \times /0.45$  objective (Olympus, Tokyo, Japan) and a xenon arc light source. The area measured with the MSP was a square (edge length  $\sim 5 \mu\text{m}$ ) that was determined by a diaphragm in the microscope's image plane. The latter was imaged at the entrance of an optical fiber connected to the detector array spectrometer. Due to the glass optics inside the microscope, the MSP spectra were limited to wavelengths  $> 360 \text{ nm}$ . However, this limitation is compensated by the bifurcated reflection probe measurements that yield a reliable signal between 250–900 nm. Note that the probe and MSP collect light from a limited aperture, and therefore the measured reflectance depends on the spatial reflection properties of the object, for instance its local flatness. All optical measurements were conducted with illumination at normal incidence.

## RESULTS

### The European Starling, *Sturnus vulgaris* Feathers, Barbules and Melanosomes

The plumage of the European starling (*S. vulgaris*) is gray-black with whitish spots, but it can prominently feature metallic blue, green or purple feather areas (**Figure 1A**). Epi-illumination light microscopy demonstrated that the colors originate from the feather barbules, which branch from either side of the barbs and partly overlap each other (**Figures 1B,C**). The barbules consist of a row of more or less flat cells, each exposing a surface with size  $\sim 30 \times 60 \mu\text{m}^2$ . The hue can differ between neighboring cells, but within a cell the hue varies only slightly, which indicates that the anatomical variation within a single barbule cell is small (**Figures 1D,E**).

As shown by electron microscopy, the barbule cell border is marked by a layer of melanosomes below a keratin cortex layer (**Figures 2A,B**). Numerous melanosomes exist in the barbule's central area, but they are randomly distributed (**Figures 2A,B**). The TEM data from previous literature yielded virtually identical values for the melanosome diameters of the green and purple barbules:  $D_m = 250 \text{ nm}$  and  $D_m = 254 \text{ nm}$ , respectively, (Durrer and Villiger, 1970). Our SEM images of cross-sectioned barbules (**Figure 2B**) also yielded similar, but slightly larger mean diameters of  $273 \pm 20 \text{ nm}$  and  $271 \pm 25 \text{ nm}$  for the green and purple barbules, respectively. The cortex thickness of the green and purple barbules varies over the width of the barbule and was estimated to be  $275 \pm 30 \text{ nm}$  and  $336 \pm 27 \text{ nm}$ , respectively.

To visualize the melanosomes of the starling's feather barbules *in situ*, we applied epi-illumination microscopy on barbules immersed in oil (**Figure 2C**). The micrographs show  $\sim 1.5 \mu\text{m}$  long, rod-shaped melanosomes, arranged in clusters that are generally oriented parallel to the barbule axis (**Figures 2C,D**; **Figure 2C** shows an example of a melanosome cluster with a deviant orientation). The micrographs yielded an interdistance

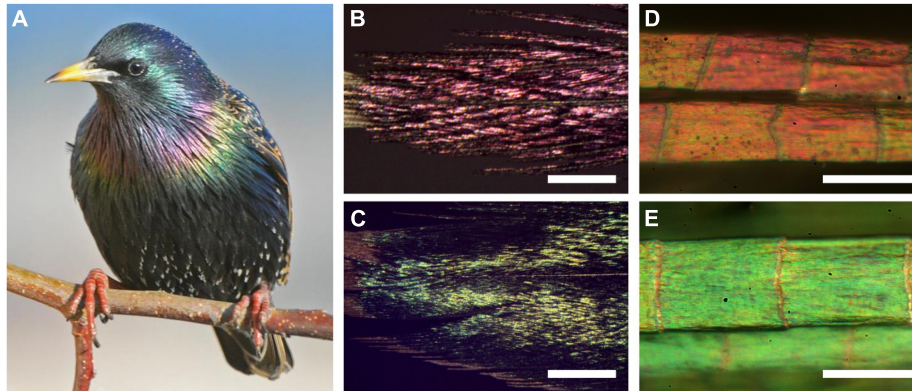


**FIGURE 1** | The European starling, *Sturnus vulgaris*, and its structural colors. **(A)** A starling with colorful throat and breast feathers (photograph by Nathan deBoer). **(B-E)** Epi-illumination light microscopy images of **(B)** a throat feather, **(C)** a breast feather, **(D)** throat barbules, and **(E)** breast barbules. Scale bars: **(B,C)** 1 mm; **(D,E)** 50  $\mu\text{m}$ .

of the melanosome rodlets in the green barbules of  $349 \pm 25$  nm and for the purple barbules  $351 \pm 22$  nm, meaning that the melanosomes are on average spaced apart by  $D_i = \sim 80$  nm.

The anatomy suggests that the barbule's cortex and melanosome layer form a simple layer-based interference reflector that causes the structural coloration. We tested this hypothesis by applying imaging scatterometry (**Figure 2F**). Local illumination of a purple barbule by a narrow aperture light beam indeed produced a scatterogram with a very restricted light spot. This signature of a very directional reflection validates the assumption. We note, however, that frequently the local scatterogram patterns deviated from an ideal, single spot. Clearly, the barbule is not flat throughout its width, as also evident from the anatomical data (**Figures 2A,B**).

### Multilayer Modeling

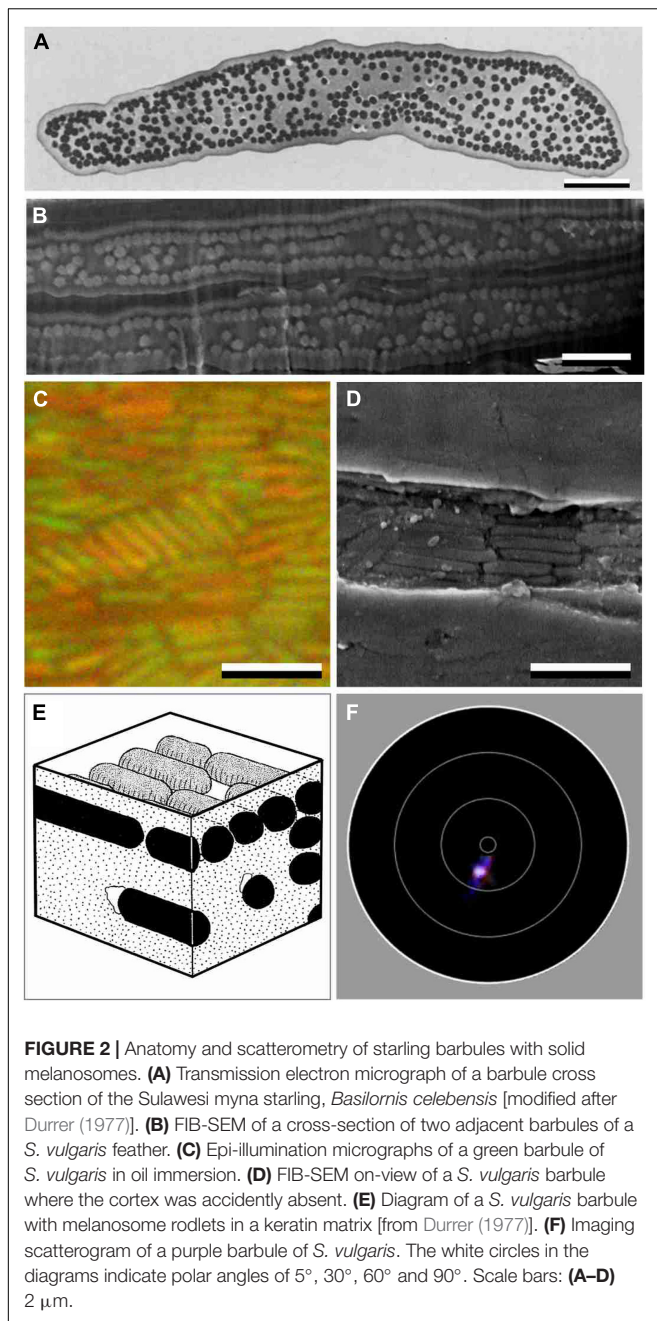
We calculated the barbule's reflectance spectra with an effective-medium-multilayer model (**Figure 3**). We treated the barbule structure as a multilayer, consisting of a keratin cortex (thickness  $c$ , facing air) and a single layer of rodlet-shaped melanosomes (diameter  $D_m$ , interdistance  $D_i$ ) in a keratin matrix (see inset of **Figure 3A**). The colored feathers differ in the thickness of the barbule cortex, as for blue-green and red-violet feathers  $c = 290$  nm and  $c = 330$  nm, respectively (**Figure 2** and Durrer and Villiger, 1970). For our initial calculations, we took for the cortex thickness  $c = 310$  nm together with a melanosome diameter  $D_m = 250$  nm as a starting point, as these values should produce reflectance values in the visible wavelength range. We used these values and the refractive indices of keratin and melanin in Eq. 1 to calculate the real and imaginary effective refractive index profiles,  $\text{Re}(\tilde{n}_{\text{eff}})$  and  $\text{Im}(\tilde{n}_{\text{eff}})$ , along the coordinate perpendicular to the barbule surface. We then investigated the influence of varying parameters within a realistic parameter range chosen to be slightly larger than the derived values.

At first, we investigated three cases, where the melanosome interdistance is  $D_i = 0, 50,$  and  $100$  nm. By applying a transfer matrix-based calculation procedure, we then obtained the reflectance and transmittance spectra (**Figures 3B,C**). The

reflectance spectra of **Figure 3B** show two distinct bands, peaking in the UV, at  $\sim 340$  nm, and in the green, at  $\sim 510$  nm. The reflectance amplitude slightly decreases with an increasing melanosome separation (**Figure 3B**), together with a slight increase of the transmittance (**Figure 3C**), but the spectral shapes hardly depend on  $D_i$ . To check the effective medium results, we performed FDTD calculations for the case  $D_m = 250$  nm,  $D_i = 0$  nm, and  $c = 310$  nm, for both TE- and TM- polarized light, yielding reflectance spectra that are virtually identical to those of **Figure 3B** (**Supplementary Figure 1**).

The transmittance increases with increasing wavelength, which is immediately recognized as the hallmark of melanin absorption. To assess the possible effect of absorption on the reflectance, we assumed that the melanin refractive index is real instead of complex. The reflectance spectrum then obtained, for the case  $D_i = 0$  (**Figure 3B**, green curve), has a slightly higher amplitude than the spectrum resulting with the complex refractive index, and its peak wavelength is a few nm shifted, but overall the effect of melanin absorption on the reflectance spectrum can be considered to be minor. When fully neglecting melanin absorption, given a reflectance of at most a few percent (**Figure 3B**), the transmittance becomes almost 100%, as expected (**Figure 3C**, green curve).

In studies of the structural coloration by melanosomes, the layers are often assumed to create discrete, stepwise changes in refractive index (see, e.g., Doucet et al., 2006). In our effective medium approach, we implemented more realistic, gradual changes in the refractive index by interpolation and thresholding with a very fine mesh. We investigated the difference between gradual and stepwise changes of the refractive index by comparing an array of contiguous solid rodlets, diameter  $D_m = 250$  nm and  $D_i = 0$  nm, with a few discrete layers, homogeneously filled with the same total amount of melanin (**Figures 3D-F**). **Figure 3D** shows the real and imaginary effective refractive index profiles for four cases: (i) the rodlets with gradually changing melanin fraction  $f_m$  with averaged melanin content  $(\pi D_m^2/4)/D_m = \pi D_m/4$ ; (ii) a discrete layer with pure melanin,  $f_m = 1$  and thickness  $\pi D_m/4$ ; (iii) a discrete layer



with reduced melanin,  $f_m = \sqrt{\pi}/2$  and thickness  $D_m\sqrt{\pi}/2$ ; (iv) a discrete layer with even less melanin,  $f_m = \pi/4$ , and thickness  $D_m$ . In all cases, the location of the center of the melanosome layers was identical (**Figure 3D**). The reflectance spectra calculated for the four cases have similar shapes and peak wavelengths ( $\sim 510$  nm) in the visible wavelength range, but the reflectance magnitudes of the extrema differ slightly (**Figure 3E**). As expected, the transmittance spectra are virtually identical, because the total melanin content is identical (**Figure 3F**).

The total melanin content is not constant when varying the diameter of the melanin rodlets (**Figures 3G–I**). We considered three cases of the melanosome diameter:  $D_m = 250$ , 300, and

350 nm, with interdistance  $D_i = 0$  nm, keeping a constant cortex thickness  $c = 310$  nm. Again, the detailed shape of the resulting reflectance spectra varies, but the spectral location of the UV stays about the same and the band in the green wavelength range (up to about 630 nm) varies only in its detailed shape (**Figure 3H**). In the long wavelength range, the reflectance peak moves bathochromic (to longer wavelengths) due to the increased optical pathlength resulting from the thicker melanin layer. Also, with an increasing rodlet diameter, the melanin content increases, causing a decrease in the transmittance (**Figure 3I**).

We finally investigated the effect of the cortex thickness. In addition to the values  $c = 290$  and 330 nm informed by EM measurements of **Figure 2B** and literature (Durrer and Villiger, 1970), we also applied slightly smaller  $c = 250$  nm and larger thicknesses  $c = 370$  nm to investigate the effect on the color response. For all cases,  $D_m = 250$  nm and  $D_i = 0$  nm are kept constant (**Figures 3J–L**). The resulting reflectance spectra have all obtained approximately the same shape, but the peak wavelengths of the four cases, 455, 496, 536, and 577 nm, respectively, are shifted  $\sim 40$  nm with respect to each other along the wavelength abscissa (**Figure 3K**). The transmittance spectra are virtually identical again (**Figure 3L**). We can conclude from the various parameter values that the cortex thickness is the most sensitive parameter that determines the barbule's reflectance spectrum and thereby its color.

### Comparison of Measured and Modeled Reflectance Spectra

We measured reflectance spectra in single cells of various colored feather barbules of *S. vulgaris* using a microspectrophotometer (MSP). **Figures 4A,B** show MSP spectra from barbule cells of a green and purple feather, respectively. Although the shape of the different spectra is similar, they are shifted with respect to each other by several tens of nm, and also the amplitude varies quite noticeably. The latter may be a consequence of the measurement procedure, because the objective of the microspectrophotometer projects a light beam with a considerable aperture onto the barbule. Since the barbule and its multilayer reflector is not perfectly flat, part of the reflected light will not be captured by the objective. In other words, even when the local cortex thickness and melanosome layer remain constant and the spectral shape thus stays the same, the amplitude of the measured reflectance will vary with the shape of the barbule surface.

In order to estimate the local cortex thicknesses, we compared two examples of measured spectra with spectra calculated with the above model. To obtain a close fit, we adjusted the parameters. Taking again  $D_m = 250$  nm, satisfactory fits for the case of a blue-green and a purple barbule were obtained with  $c = 300$  nm and  $c = 390$  nm, respectively, (**Figure 4C**).

Whereas the reflectance spectra measured locally from within a single barbule cell area vary (**Figures 4A,B**), the coloration observed visually will be the sum of local reflection spectra. This can be illustrated by measuring the reflectance with a bifurcated probe, which integrates the reflections from an area on the order of  $1 \text{ mm}^2$ . The different colored feather areas then yield clearly distinct reflectance spectra (**Figure 4D**).

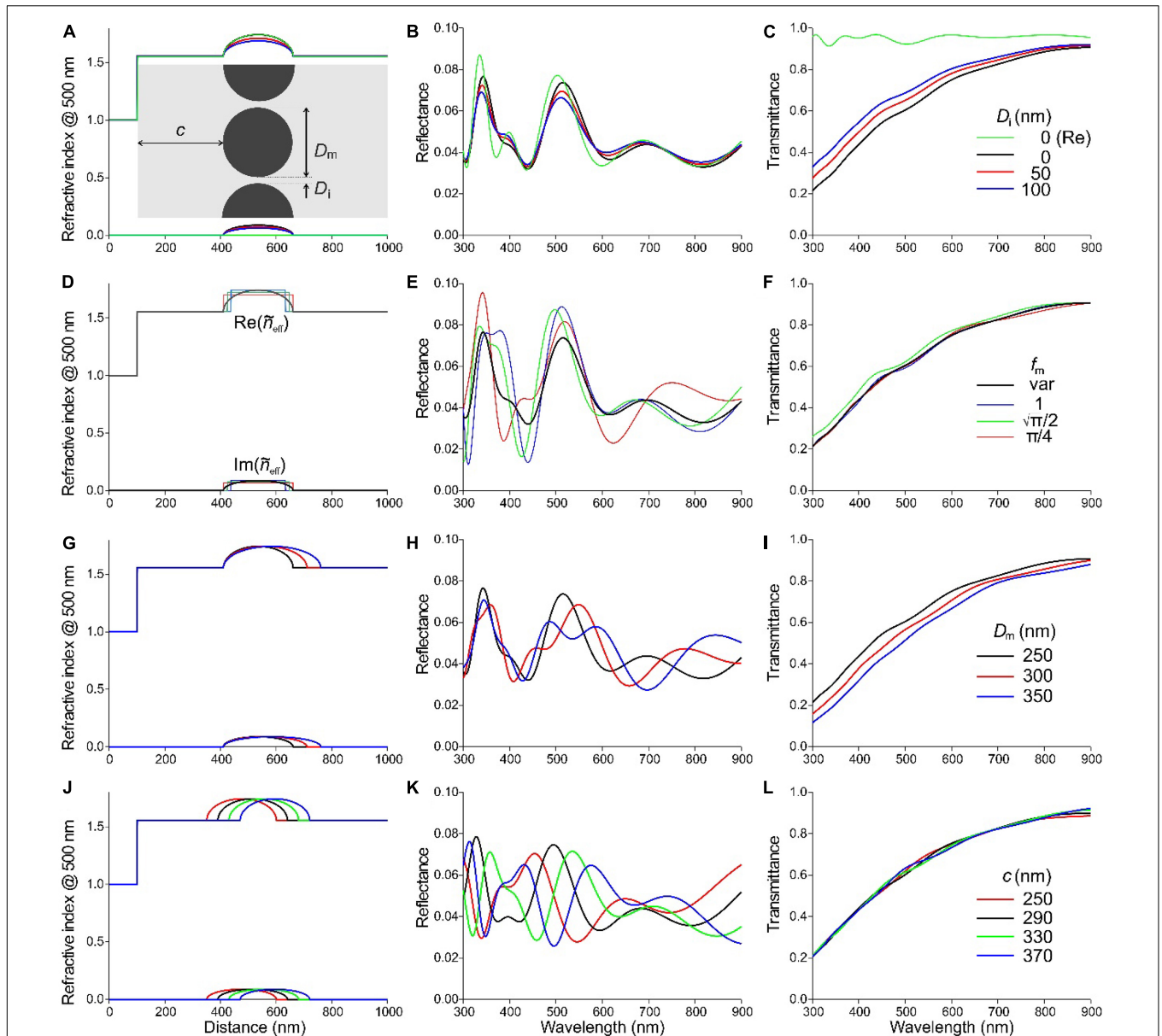


**FIGURE 3 |** Effective-medium-multilayer modeling of a *S. vulgaris* barbule. **(A–C)** Rodlet melanosomes with diameter  $D_m = 250$  nm and interdistance  $D_i = 0, 50,$  and  $100$  nm embedded in a keratin barbule at a distance  $c = 310$  nm from the border. In the legend of **(C)**, (Re) concerns the case where the refractive index is real, i.e., the melanin is absorptionless. **(D–F)** The case of a layer of rodlet melanosomes with varying melanin fraction ( $f_m$  var) compared with discrete melanin layers of different melanin fraction and layer thickness (see text for details). **(G–I)** Melanosomes with diameter  $D_m = 250, 300,$  and  $350$  nm. **(J–L)** Layer of melanosomes, diameter  $D_m = 250$  nm, interdistance  $D_i = 0$  nm, with cortex thickness  $c = 250, 290, 330,$  and  $370$  nm. **(A, D, G, J)** Profiles of the real and imaginary refractive index at  $500$  nm. The barbule (and cortex) surface is at abscissa (distance) value  $100$  nm. **(B, E, H, K)** Reflectance spectra. **(C, F, I, L)** Transmittance spectra.

## Feathers of the Cape Starling, *Lamprolornis nitens*

### Feathers, Barbules and Melanosomes

Compared to the European starling, the Cape starling (*L. nitens*) has a much more impressive coloration, with striking metallic colors throughout its entire iridescent plumage (Figure 5A). The head, body and wing feathers are colored variously blue-green (Figure 5B), while the tail is uniformly blue (Figure 5C). Micrographs show that individual barbule cells are again rather

uniformly colored, but the color of adjacent cells can differ substantially (Figures 5D,E).

The Cape starling has hollow melanosomes (Craig and Hartley, 1985; Maia et al., 2013). A transmission electron micrograph of a barbule cross-section of a related glossy starling, the Superb starling *Lamprolornis superbus*, shows a single layer of hollow melanosomes, which line the entire barbule perimeter like the melanosomes of *S. vulgaris* barbules; in the barbule interior some randomly arranged hollow melanosomes are seen

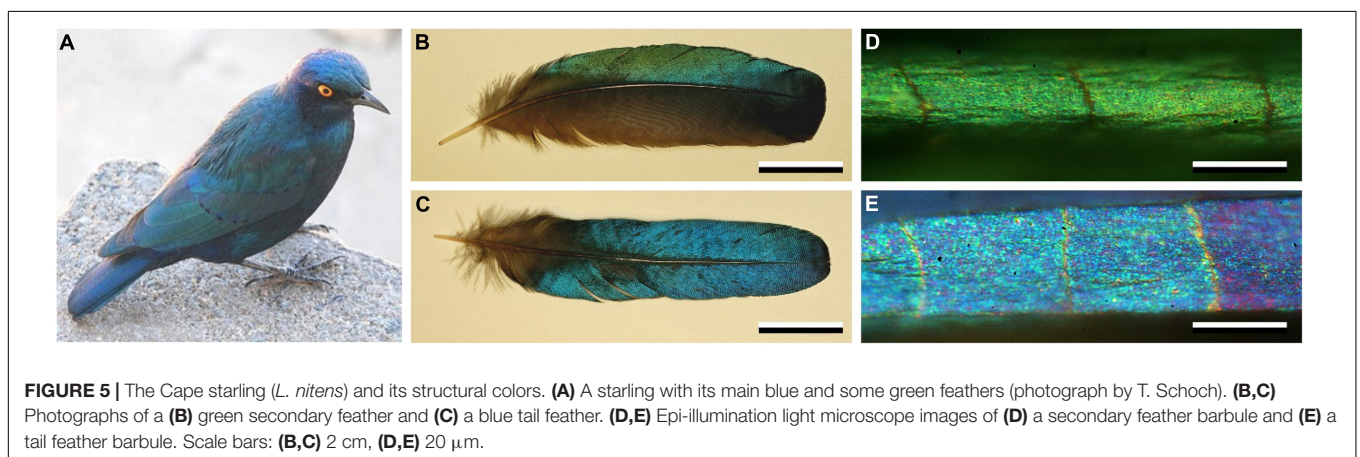
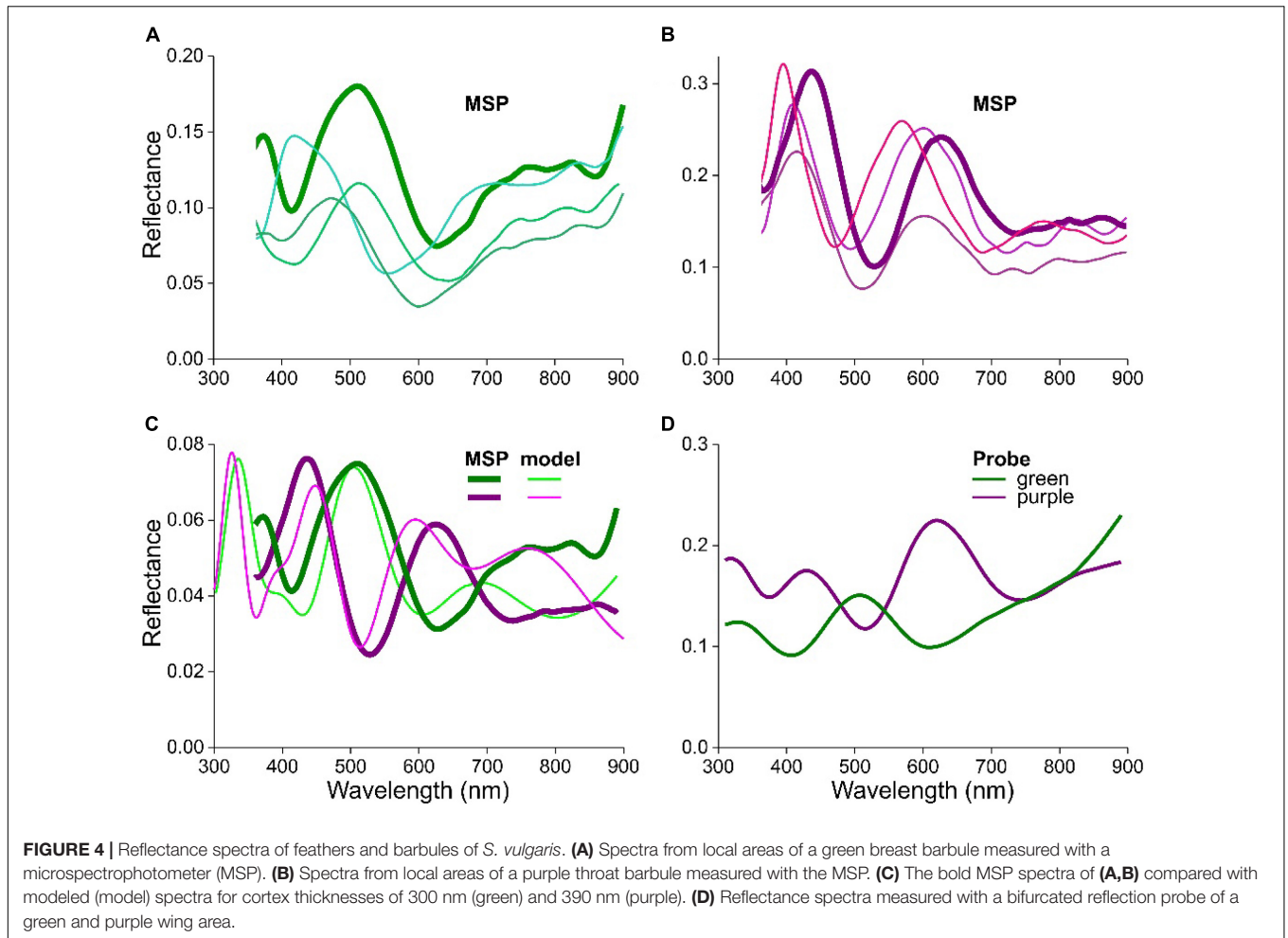
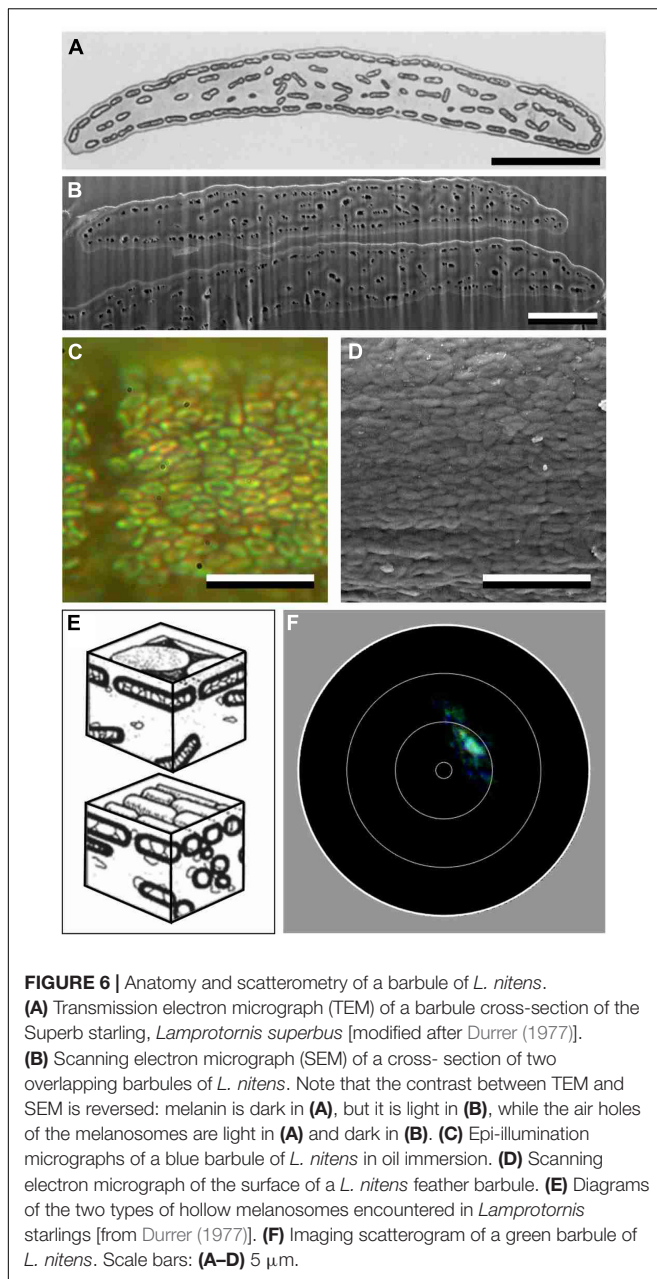


[**Figure 6A**; from Durrer and Villiger (1970)]. Scanning electron micrographs of cross-sections of the investigated *L. nitens* barbules show essentially the same organization (**Figure 6B**) and gives a cortex thickness of about  $118 \pm 25$  and  $185 \pm 31$  nm for the blue and the green barbule, respectively.

Durrer and Villiger described the melanosomes of four *Lamprolornis* species as platelet-shaped, with a compact melanin

sheet that envelops a honeycomb-like air-filled space (Durrer and Villiger, 1970). Epi-illumination microscopy on feather barbules of *L. nitens* immersed in oil visualized the melanosomes (**Figure 6C**). The resulting images differed remarkably from those of the European starling in that they show a distribution of different melanosome shapes with a majority of doughnut-like shapes intermingled with small bars. These different shapes were



also visible in scanning electron micrographs of the surface of an *L. nitens* feather barbule (Figure 6D).

The immersion images suggest that the melanosomes are less uniform in size and shape than the melanosomes of *S. vulgaris*. The images show the appearance of bars and doughnut-like shapes in Figures 6C,D, which might either suggest a mixture of melanosome shapes ranging between rodlets and platelets (Figure 6E), or a disordered arrangement of platelets alone. An extensive comparative study on the melanosomes of African starlings demonstrated that the melanin granules of *Lamprolornis* may be short and thick as well as slender and elongated (Craig and Hartley, 1985). Evolutionary transitions between rodlets and platelets have been recently suggested for starlings

(Maia et al., 2013; Rubenstein et al., 2021). Furthermore, the interior of the melanosomes is presumably not fully hollow as TEM studies showed the existence of minor cross-linking elements (Figure 6E).

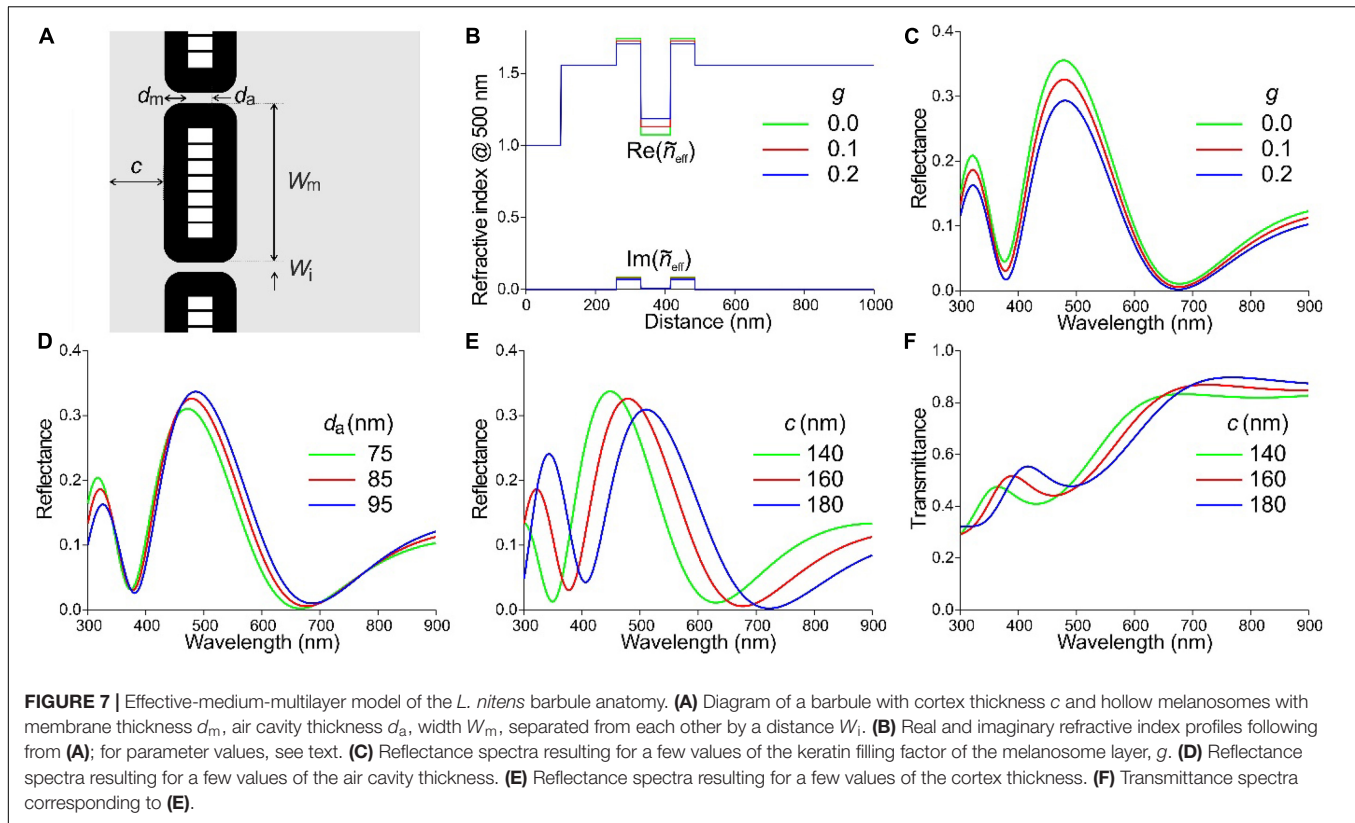
Whatever the fine structure, the single layer of melanosomes together with the keratin cortex will create a multilayer reflector. We investigated this by mounting a blue feather piece in the imaging scatterometer. Narrow beam illumination of a small barbule area yielded a quite discrete spot, demonstrating that locally the barbule indeed approximates an ideal reflector (Figure 6F). Similar as with the European starling, we often obtained scatterograms with more distributed patterns, indicating a varying flatness of the barbules' multilayers.

### Multilayer Modeling

For the modeling of the reflectance spectra, we used anatomical data of the feathers of the Lesser blue-eared glossy-starling, *L. chloropterus*, as it is closely related to *L. nitens* and similarly colored (Durrer and Villiger, 1970; Craig and Hartley, 1985; Maia et al., 2013) in addition to the EM data of the investigated cross-sections. Figure 7A presents a diagram of a barbule with cortex thickness  $c$  and cylindrical, hollow melanosomes, membrane thickness  $d_m$ , air cavity thickness  $d_a$ , and width  $W_m$ , separated from each other by a distance  $W_i$ . For the modeling we used  $d_m = 70$  nm and  $d_a = 85$  nm (Figure 6; Durrer and Villiger, 1970). We first investigated the effect on the reflectance of an incomplete filling of the melanosome layer. For our initial calculations we took for the cortex thickness  $c = 160$  nm, and we assumed, based on the electron micrographs, that the honeycomb of thin melanin membranes within the air cavities take up 10% of the volume, so that the inside air fraction is 0.9. The keratin filling factor of the melanosome layer  $g = W_i/W_m$  has the value  $g = 0$  when the melanosomes touch each other. With an increase of the filling factor to  $g = 0.1$  and  $g = 0.2$ , the refractive index contrast of the melanosome layer decreases, as shown in the refractive index profiles (Figure 7B). The calculated reflectance spectra show that this causes a decrease of the reflectance amplitude, but the peak wavelength remains virtually the same (Figure 7C).

We subsequently considered a change in the air cavity thickness from 75 to 95 nm (well sampling the range reported for various *Lamprolornis* species of 73 to 98 nm; Durrer and Villiger, 1970). This causes slight changes in both the amplitude and peak wavelength of the reflectance spectra ( $\lambda_{\text{max}}$ ), but their shape remains about the same (Figure 7D). For  $d_a = 75, 85, 95$  nm,  $\lambda_{\text{max}} = 472, 479, \text{ and } 486$  nm, respectively, i.e., a 10 nm increase of the air cavity thickness causes a 7 nm peak wavelength shift (Figure 7D).

To underscore the effective medium results, we performed FDTD calculations for the case  $d_m = 70$  nm,  $d_a = 85$  nm, and  $c = 160$  nm, for both TE- and TM-polarized light (Supplementary Figure 2). The calculated TE- and TM-reflectance spectra slightly differ in amplitude, demonstrating the effect of anisotropy of the melanosomes. Nevertheless, the reflectance spectra obtained for different filling factors with effective-medium-multilayer modeling and FDTD were virtually identical (Figure 7C and Supplementary Figure 2).



Changes in the cortex thickness again have a substantial effect on the reflectance spectra (**Figure 7E**). For  $c = 140, 160$  and  $180$  nm, the peak wavelength is  $\lambda_{\max} = 449, 480$ , and  $511$  nm, respectively, i.e., an increase of the cortex thickness by  $20$  nm causes a  $31$  nm peak wavelength shift. **Figure 7F** shows the related transmittance spectra, where the melanin absorption spectrum is still well recognizable, but the transmittance in the blue-green wavelength range is reduced due to the higher reflectance in this band.

### Comparison of Measured and Modeled Reflectance Spectra

We measured reflectance spectra of the variously colored feather barbules of *L. nitens* with a microspectrophotometer (MSP) on local areas of single barbule cells. **Figures 8A,B** show MSP spectra from single barbule cells of a blue and green feather, respectively. As in the case of the European starling, the shape of the various spectra is similar, but their spectral location somewhat differs, and even more their amplitudes. This will again be due to the dependence on the local barbule shape as well as the multilayer dimensions.

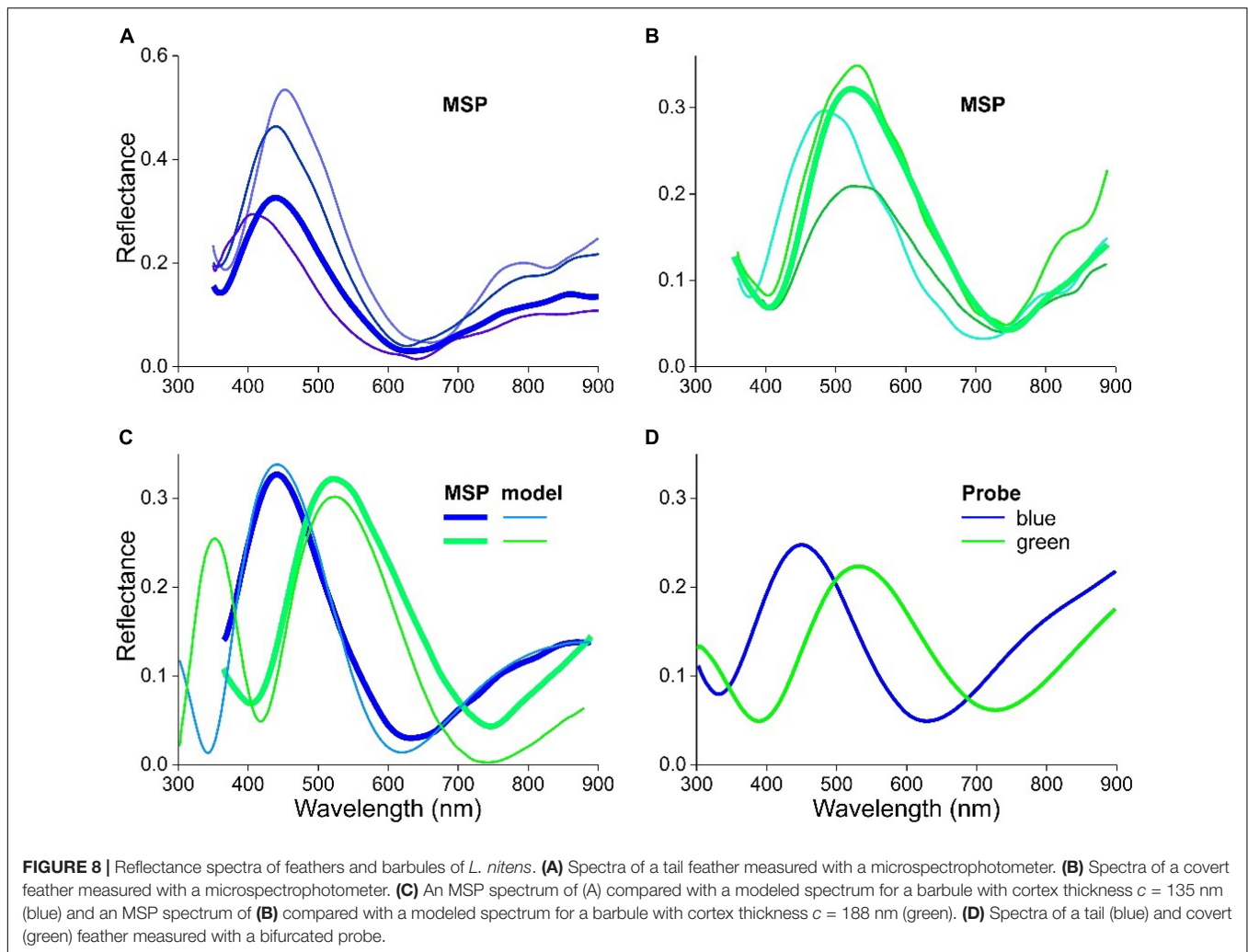
We compared two of the measured spectra with spectra following from optical modeling. Satisfactory fits were obtained for the tail feather barbules using a cortex thickness  $c = 135$  nm and for the covert feather barbules  $c = 188$  nm (**Figure 8C**). Nearly identical fits to the different color spectra of *L. nitens* could also be obtained by changing the melanosome air cavity thickness and/or the melanin membrane thickness, but the necessary

parameter variation was larger for the air cavity thickness and the melanin membrane thickness than the  $53$  nm change that was necessary in cortex thickness variation. This would be beyond the range reported in the literature. We furthermore measured reflectance spectra of the tail and covert feathers of *L. nitens* with a bifurcated reflection probe (**Figure 8D**). The spectra are representative for the observed colors and closely resemble the averaged reflectance spectra of **Figures 8A,B**.

## DISCUSSION

Here we performed a study on two starling species that combines optical modeling and direct optical and ultrastructural measurements on the barbules of starling feathers that contain a single layer of melanosomes. The experimentally obtained reflectance spectra could be interpreted well with effective-medium-multilayer modeling (**Figures 4C, 8C**). In the optical modeling, we treated the barbules as containing a cortex with a single melanosome layer. However, the barbule interior contains randomly located melanosomes, which will contribute to the reflectance, because they will scatter light transmitted by the cortex-melanosome layers.

The transmittance calculations show that already a single melanosome layer considerably reduces the transmittance throughout the visible wavelength range. Consequently, the melanosomes of the barbule interior may somewhat enhance the reflectance in the longer wavelength range but they will also further reduce the transmittance at all wavelengths. A further



contribution to the barbule reflectance could originate from the melanosome layer and cortex at the barbule's underside. However, the fraction of the light flux that is transmitted by the upper multilayer, passes through the interior and then is reflected (firstly) at the lower multilayer layers and (secondly) at the barbule's underside will be very minor. In other words, already with a monolayer of melanosomes near the barbule boundary, the reflectance is set by the layer on the illuminated side. Similarly, previous studies on mallard and magpie feathers, which have barbules with several layers of melanosomes on both sides of the barbules, demonstrated that the upper stack determines the barbule reflectance (Stavenga et al., 2017, 2018).

In a thin-film modeling study on blue-black grassquit feather barbules, where a keratin layer overlies a single melanin layer, Maia et al. (2009) similarly, concluded that a keratin layer above a melanin layer mainly determines the reflectance spectrum. Furthermore, a study on tree swallow barbules indicated that humidity-induced reflectance changes resulted from a modified cortex thickness (Eliason and Shawkey, 2010). Also, in a comparative study on a large number of bird species with matte

and glossy plumage, Maia and colleagues emphasized the role of the keratin layer when the feather barbules have a single layer of melanosomes. Using thin film modeling, the authors concluded that a keratinous cortex thickness of 110–180 nm together with a melanosome layer with thickness greater than 115 nm causes glossy feathers (Maia et al., 2011). In these previous studies on bird feather coloration, the refractive indices of keratin and melanin were assumed to be wavelength-independent, and the real part of the refractive index of melanin of 2.0 was used. In the present study, we implemented the recently measured wavelength-dependent refractive index values of the different feather components, where the real part decreases from 1.8 to 1.7 for melanin (Leertouwer et al., 2011; Stavenga et al., 2015). The excessively high melanin refractive index used in the previous studies hence has not gravely affected the results for a single melanin layer, but will have larger implications for the optical function of more complex photonic multilayer structures (Wilts et al., 2014).

A high refractive index contrast is caused by the air compartments in the hollow melanosomes of *L. nitens*, which thus realizes a much higher barbule reflectance compared to

*S. vulgaris*. Hollow melanosomes therefore might have been selected in *L. nitens* due to the intensely directional appearance they generate. Since the exact dimensions of the melanosomes are again less relevant than the cortex thickness (Figures 7C,D), the keratin cortex most effectively determines the location of the spectral peaks (Figure 7E).

Our present measurements as well as modeling were only performed for normally incident light. The feather colors will depend on the angle of illumination or observation, due to the layered structure of the feathers, which causes iridescence. A hypsochromic shift of the reflectance spectra will occur with increasing angle of light incidence, as is amply shown in related papers (see, e.g., Eliason and Shawkey, 2012; Stavenga, 2014; Xiao et al., 2014). Accordingly, illumination with a wide-aperture light source, which was the case in the experiments with an oil immersion objective (Figures 2C, 6C), will cause a strongly broadened reflectance spectrum and thus a color strongly differing from that seen with a low power objective (Figures 1, 5).

*Sturnus vulgaris* has iridescent feathers containing solid melanosomes in a small part of the modestly shiny plumage, but *L. nitens* has barbules with hollow melanosomes in most feathers, which likely causes its strikingly glossy, iridescent plumage. Whether and how local irregularities will influence the iridescence will need to be further investigated. This will entail the assembly of quantitative anatomical data of the cortex and melanosome dimensions, but we expect that this data will not essentially change our insight into the principal function of the keratin cortex in determining the peak wavelength of the reflectance bands.

Whereas the plumage of the European starling is modestly colored and speckled, the plumage of the Cape starling is uniformly colored and strikingly directional. The iridescent plumage coloration can have various biological functions, for instance as a display for conspecifics or as camouflage against predators. It is therefore interesting to compare the starling colors with the spectral sensitivities of their photoreceptors. The four classes of photoreceptors of *S. vulgaris*, UVS, SWS, MWS, and LWS, are known to have sensitivity peak wavelengths at 369, 453, 545, and 607 nm, respectively, (Hart and Vorobyev, 2005). The reflectance spectra of the blue and green feathers of the Cape starling (Figure 8D) correspond to the sensitivity spectra of the SWS and MWS photoreceptors, but a similar correspondence is not immediately apparent for the European starling feathers. In fact, the spectra of Figure 4D are two examples of a broad continuum, as can also be seen from the variously colored feathers of the starling shown in Figure 1A.

The starlings, Sturnidae, constitute a large family of passerine birds that have structural-colored feathers, employing a remarkably wide variety of melanosomes that are arranged in diverse ways. This includes solid and hollow rodlets as well as solid and hollow platelets, which are mostly arranged in a single layer but also in a multilayer stack (Durrer and Villiger, 1970; Craig and Hartley, 1985; Maia et al., 2013). In the case of a large stack of melanosomes, the stack

periodicity is responsible for the peak wavelength and the shape of the reflectance spectra (Eliason et al., 2013). Durrer and Villiger (1970) assumed that a single melanosome layer determines the feather color, particularly for structures with hollow melanosomes. We find in our modeling that the cortex thickness is a key factor in determining the feather colors. While the diameter of the solid melanosomes in the *S. vulgaris* seems to be unimportant, the hollow melanosomes in *L. nitens* crucially cause the high reflectance amplitude. Our findings can have implications also for the design of novel bio-inspired materials, e.g., by informing bio-inspired approaches to tune color with the use of a single sensing layer (Isapour and Lattuada, 2018).

Even in the presence of a large stack of melanosomes that form a multilayer, the keratin cortex can play a special role. This is for instance the case in the breast feathers of the bird of paradise *Parotia lawesii*. Their barbules contain a multilayer of solid melanin rodlets that creates a golden reflection. The layers are arranged skew to the enveloping cortex, and as a consequence the light beams reflected by the cortex and the multilayer become separated. For the light reflected by the cortex, the melanin rodlets then act together as a high refractive index medium as well as a strong absorber, and the cortex here acts as an independent blue-reflecting thin film (Stavenga et al., 2011; Wilts et al., 2014). Furthermore, in hummingbird feathers, where the barbules have large stacks of hollow platelet melanosomes, the cortex appears to importantly modulate the feather reflectance spectra (Eliason et al., 2020); for similar effects in the jewel beetle, see Yoshioka et al. (2012).

In conclusion, the two starling species, with a single layer of melanosomes in their feather barbules, demonstrate that the spectral position of the reflectance bands can be simply tuned by adjusting the cortex thickness. In both studied species, the variously colored feathers appeared to have an identical arrangement of melanosomes, but when the melanosomes are hollow, the reflectance is greatly enhanced. The wide variety of arrangements of solid or hollow melanosomes, embedded in the keratin matrix of bird feather barbules, demonstrates the large flexibility birds have in realizing their subdued or extravagant structural colors.

## DATA AVAILABILITY STATEMENT

The raw data supporting the conclusions of this article will be made available by the authors, without undue reservation.

## AUTHOR CONTRIBUTIONS

All authors performed the measurements and modeling and wrote the manuscript.

## FUNDING

This study was financially supported by the Ph.D. scholarship programme of the University of Groningen and the Advanced Materials research program of the Zernike National Research Centre under the Bonus Incentive Scheme of the Dutch Ministry for Education, Culture and Science (to PF), by the Swiss National Science Foundation through the National Center of Competence in Research Bio-Inspired Materials and the Ambizione Programme (168223 to BW), and the Air Force Office of Scientific Research/European Office of Aerospace Research and Development AFOSR/EOARD (grant FA9550-15-1-0068 to DS).

## REFERENCES

- Craig, A. J., and Hartley, A. H. (1985). The arrangement and structure of feather melanin granules as a taxonomic character in African starlings (Sturnidae). *Auk* 102, 629–632.
- D'Alba, L., Kieffer, L., and Shawkey, M. D. (2012). Relative contributions of pigments and biophotonic nanostructures to natural color production: a case study in budgerigar (*Melopsittacus undulatus*) feathers. *J. Exp. Biol.* 215, 1272–1277. doi: 10.1242/jeb.064907
- Doucet, S. M., Shawkey, M. D., Hill, G. E., and Montgomerie, R. (2006). Iridescent plumage in satin bowerbirds: structure, mechanisms and nanostructural predictors of individual variation in colour. *J. Exp. Biol.* 209, 380–390. doi: 10.1242/jeb.01988
- Durrer, H. (1965). Bau und Bildung der Augfeder des Pfaus *Pavo cristatus* L. *Rev. Suisse Zool* 72, 264–411.
- Durrer, H. (1977). Schillerfarben der Vogelfeder als Evolutionsproblem. *Denkschr. Schweiz. Naturforsch. Ges.* 91, 1–126.
- Durrer, H. (1986). "Colouration," in *Biology of the Integument*, eds J. Bereiter-Hahn, A. G. Matoltsky, and K. Richards (Berlin: Springer), 239–247.
- Durrer, H., and Villiger, W. (1966). Schillerfarben der Trogoniden. *J. Ornithol.* 107, 1–26. doi: 10.1007/bf01671870
- Durrer, H., and Villiger, W. (1970). Schillerfarben der Stare (Sturnidae). *J. Ornithol.* 111, 133–153.
- Eliason, C. M., and Shawkey, M. D. (2010). Rapid, reversible response of iridescent feather color to ambient humidity. *Opt. Express* 18, 21284–21292. doi: 10.1364/OE.18.021284
- Eliason, C. M., and Shawkey, M. D. (2012). A photonic heterostructure produces diverse iridescent colours in duck wing patches. *J. R. Soc. Interface* 9, 2279–2289. doi: 10.1098/rsif.2012.0118
- Eliason, C. M., Bitton, P. P., and Shawkey, M. D. (2013). How hollow melanosomes affect iridescent colour production in birds. *Proc. R. Soc. B* 280:20131505. doi: 10.1098/rspb.2013.1505
- Eliason, C. M., Maia, R., Parra, J. L., and Shawkey, M. D. (2020). Signal evolution and morphological complexity in hummingbirds (Aves: Trochilidae). *Evolution* 74, 447–458. doi: 10.1111/evo.13893
- Freyer, P., and Stavenga, D. G. (2020). Biophotonics of diversely coloured peacock tail feathers. *Faraday Discuss.* 223, 49–62. doi: 10.1039/d0fd00033g
- Freyer, P., Wilts, B. D., and Stavenga, D. G. (2019). Reflections on iridescent neck and breast feathers of the peacock, *Pavo cristatus*. *Interface Focus* 9:20180043. doi: 10.1098/rsfs.2018.0043
- Giraldó, M. A., Parra, J. L., and Stavenga, D. G. (2018). Iridescent colouration of male Anna's hummingbird (*Calypte anna*) caused by multilayered barbules. *J. Comp. Physiol. A* 204, 965–975. doi: 10.1007/s00359-018-1295-8
- Greenewalt, C. H., Brandt, W., and Friel, D. D. (1960). Iridescent colors of hummingbird feathers. *J. Opt. Soc. Am.* 50, 1005–1013. doi: 10.1364/josa.50.001005
- Gruson, H., Elias, M., Andraud, C., Djediat, C., Berthier, S., Doutrelant, C., et al. (2019). Hummingbird iridescence: an unsuspected structural diversity

## ACKNOWLEDGMENTS

We thank H. L. Leertouwer for providing excellent technical support and C. J. van der Kooi and the reviewers for critical reading of the manuscript.

## SUPPLEMENTARY MATERIAL

The Supplementary Material for this article can be found online at: <https://www.frontiersin.org/articles/10.3389/fevo.2021.746254/full#supplementary-material>

- influences colouration at multiple scales. *bioRxiv* [Preprint] doi: 10.1101/699744
- Hart, N. S., and Vorobyev, M. (2005). Modelling oil droplet absorption spectra and spectral sensitivities of bird cone photoreceptors. *J. Comp. Physiol. A* 191, 381–392.
- Hill, G. E., and McGraw, K. J. (2006). *Bird Coloration. Vol. 1: Mechanisms and Measurements*. Cambridge, MA: Harvard University Press.
- Isapour, G., and Lattuada, M. (2018). Bioinspired stimuli-responsive color-changing systems. *Adv. Mat.* 30:1707069. doi: 10.1002/adma.201707069
- Kinoshita, S. (2008). *Structural Colors in the Realm Of Nature*. Singapore: World Scientific.
- Leertouwer, H. L., Wilts, B. D., and Stavenga, D. G. (2011). Refractive index and dispersion of butterfly scale chitin and bird feather keratin measured by interference microscopy. *Opt. Express* 19, 24061–24066. doi: 10.1364/OE.19.024061
- Maia, R., Caetano, J. V. O., Bao, S. N., and Macedo, R. H. (2009). Iridescent structural colour production in male blue-black grassquit feather barbules: the role of keratin and melanin. *J. R. Soc. Interface* 6, S203–S211. doi: 10.1098/rsif.2008.0460.focus
- Maia, R., D'Alba, L., and Shawkey, M. D. (2011). What makes a feather shine? A nanostructural basis for glossy black colours in feathers. *Proc. R. Soc. B* 278, 1973–1980. doi: 10.1098/rspb.2010.1637
- Maia, R., Rubenstein, D. R., and Shawkey, M. D. (2013). Key ornamental innovations facilitate diversification in an avian radiation. *Proc. Natl. Acad. Sci. U.S.A.* 110, 10687–10692. doi: 10.1073/pnas.1220784110
- Mason, C. W. (1923). Structural colors in feathers. *J. Phys. Chem.* 27, 401–447. doi: 10.1021/j150230a001
- McGraw, K. J. (2006). "Mechanics of uncommon colors: pterins, porphyrins and psittacofulvins," in *Bird Coloration, Vol. 1, Mechanisms and Measurements*, eds G. E. Hill and K. J. McGraw (Cambridge, MA: Harvard University Press), 354–398.
- Prum, R. O. (2006). "Anatomy, physics, and evolution of avian structural colors," in *Bird Coloration, Vol. 1, Mechanisms and Measurements*, eds G. E. Hill and K. J. McGraw (Cambridge, MA: Harvard University Press), 295–353.
- Rubenstein, D. R., Corvelo, A., MacManes, M. D., Maia, R., Narzisi, G., Rousaki, A., et al. (2021). Feather gene expression elucidates the developmental basis of plumage iridescence in African starlings. *J. Hered.* 112, 417–429. doi: 10.1093/jhered/esab014
- Shawkey, M. D., and D'Alba, L. (2017). Interactions between colour-producing mechanisms and their effects on the integumentary colour palette. *Phil. Trans. R. Soc. B* 372, 20160536. doi: 10.1098/rstb.2016.0536
- Stavenga, D. G. (2014). Thin film and multilayer optics cause structural colors of many insects and birds. *Mat. Today Proc.* 1, 109–121. doi: 10.1016/j.matpr.2014.09.007
- Stavenga, D. G., Leertouwer, H. L., Piri, P., and Wehling, M. F. (2009). Imaging scatterometry of butterfly wing scales. *Opt. Express* 17, 193–202.
- Stavenga, D. G., Leertouwer, H. L., Marshall, N. J., and Osorio, D. C. (2011). Dramatic colour changes in a bird of paradise caused by uniquely structured breast feather barbules. *Proc. R. Soc. B* 278, 2098–2104. doi: 10.1098/rspb.2010.2293

- Stavenga, D. G., Leertouwer, H. L., Osorio, D. C., and Wilts, B. D. (2015). High refractive index of melanin in shiny occipital feathers of a bird of paradise. *Light Sci. Appl.* 4:e243. doi: 10.1038/lsa.2015.16
- Stavenga, D. G., Leertouwer, H. L., and Wilts, B. D. (2018). Magnificent magpie colours by feathers with layers of hollow melanosomes. *J. Exp. Biol.* 221:174656. doi: 10.1242/jeb.174656
- Stavenga, D. G., van der Kooi, C. J., and Wilts, B. D. (2017). Structural coloured feathers of mallards act by simple multilayer photonics. *J. R. Soc. Interface* 14, 10.1098. doi: 10.1098/rsif.2017.0407
- Tinbergen, J., Wilts, B. D., and Stavenga, D. G. (2013). Spectral tuning of Amazon parrot feather coloration by psittacofulvin pigments and spongy structures. *J. Exp. Biol.* 216, 4358–4364. doi: 10.1242/jeb.091561
- Wilts, B. D., Leertouwer, H. L., and Stavenga, D. G. (2009). Imaging scatterometry and microspectrophotometry of lycaenid butterfly wing scales with perforated multilayers. *J. R. Soc. Interface* 6, S185–S192. doi: 10.1098/rsif.2008.0299.focus
- Wilts, B. D., Michielsen, K., De Raedt, H., and Stavenga, D. G. (2014). Sparkling feather reflections of a bird-of-paradise explained by finite-difference time-domain modeling. *Proc. Natl. Acad. Sci. U.S.A.* 111, 4363–4368. doi: 10.1073/pnas.1323611111
- Xiao, M., Dhinojwala, A., and Shawkey, M. (2014). Nanostructural basis of rainbow-like iridescence in common bronzewing Phaps chalcoptera feathers. *Opt. Express* 22, 14625–14636. doi: 10.1364/OE.22.014625
- Xiao, M., Shawkey, M. D., and Dhinojwala, A. (2020). Bioinspired melanin-based optically active materials. *Adv. Opt. Mat.* 8:2000932. doi: 10.3390/nano10112276
- Yeh, P. (2005). *Optical Waves in Layered Media*. Hoboken NJ: Wiley-Interscience.
- Yoshioka, S., Kinoshita, S., Iida, H., and Hariyama, T. (2012). Phase-adjusting layers in the multilayer reflector of a jewel beetle. *J. Phys. Soc. Jpn.* 81:054801.
- Zi, J., Yu, X. D., Li, Y. Z., Hu, X. H., Xu, C., Wang, X. J., et al. (2003). Coloration strategies in peacock feathers. *Proc. Natl. Acad. Sci. U.S.A.* 100, 12576–12578.

**Conflict of Interest:** The authors declare that the research was conducted in the absence of any commercial or financial relationships that could be construed as a potential conflict of interest.

**Publisher's Note:** All claims expressed in this article are solely those of the authors and do not necessarily represent those of their affiliated organizations, or those of the publisher, the editors and the reviewers. Any product that may be evaluated in this article, or claim that may be made by its manufacturer, is not guaranteed or endorsed by the publisher.

Copyright © 2021 Freyer, Wilts and Stavenga. This is an open-access article distributed under the terms of the Creative Commons Attribution License (CC BY). The use, distribution or reproduction in other forums is permitted, provided the original author(s) and the copyright owner(s) are credited and that the original publication in this journal is cited, in accordance with accepted academic practice. No use, distribution or reproduction is permitted which does not comply with these terms.